
TinyBayes: Closed-Form Bayesian Inference via Jacobi Prior for Real-Time Image Classification on Edge Devices

Shouvik Sardar*
Data Science Group
Chennai Mathematical Institute
ORCID: 0009-0004-0550-0271

Sourish Das
Data Science Group
Chennai Mathematical Institute
ORCID: 0000-0002-5354-6520

Abstract

Cocoa (*Theobroma cacao*) is a critical cash crop for millions of smallholder farmers in West Africa, where Cocoa Swollen Shoot Virus Disease (CSSVD) and anthracnose cause devastating yield losses. Automated disease detection from leaf images is essential for early intervention, yet deploying such systems in resource-constrained settings demands models that are small, fast, and require no internet connectivity. Existing edge-deployable plant disease systems rely on end-to-end deep learning without uncertainty quantification, while Bayesian methods for edge devices focus on hardware-level inference architectures rather than agricultural applications. We bridge this gap with TinyBayes, the first framework to combine a closed-form Bayesian classifier with a mobile-grade computer vision pipeline for crop disease detection. Our pipeline uses YOLOv8-Nano (5.9 MB) for lesion localisation, MobileNetV3-Small (3.5 MB) for feature extraction, and the Jacobi prior; a Bayesian method that provides exact, non-iterative estimators via projection; for classification. The Jacobi-DMR (Distributed Multinomial Regression) classifier adds only 13.5 KB to the pipeline, bringing the total model size within 9.5 MB, while achieving 78.7% accuracy on the Amini Cocoa Contamination Challenge dataset and enabling end-to-end CPU inference under 150 ms per image. We benchmark against seven classifiers including Random Forest, SVM, Ridge, Lasso, Elastic Net, XGBoost, and Jacobi-GP, and demonstrate that the Jacobi-DMR offers the best trade-off between accuracy, model size, and inference speed for edge deployment. We have proved the asymptotic equivalence and consistency, asymptotic normality and the bias correction of Jacobi-DMR. All data and codes are available here: <https://github.com/shouvik-sardar/TinyBayes>

1 Introduction

Cocoa (*Theobroma cacao* L.) underpins a global industry worth over \$130 billion annually, with more than 60% of production concentrated in West Africa [International Cocoa Organization, 2023]. Smallholder farmers, who account for the vast majority of cocoa cultivation, face persistent threats from plant diseases. Cocoa Swollen Shoot Virus Disease (CSSVD), transmitted by mealybugs, causes leaf swelling, shoot dieback, and eventual tree death with no known cure [Dzahini-Obiatey et al., 2010]. Anthracnose, caused by *Colletotrichum* species, produces necrotic lesions that reduce both yield and bean quality [Marelli et al., 2019]. Traditional identification by trained extension officers is slow, expensive, and inaccessible in remote regions.

*Correspondence to sardar@cmi.ac.in

Recent advances in computer vision have enabled automated plant disease detection [Mohanty et al., 2016]. However, deploying deep learning models in Sub-Saharan Africa faces three practical constraints: (i) limited computational resources on farmers’ entry-level smartphones, (iii) very patchy to no-internet connectivity; and (ii) the need for uncertainty quantification to support reliable decision-making. These constraints define three active but largely disjoint research threads.

The first thread, *TinyML for agriculture*, applies lightweight architectures such as MobileNet and quantised models to on-device plant disease classification [Malche et al., 2026]. These systems are computationally efficient but lack any Bayesian component, offering point predictions without uncertainty estimates.

The second thread, *Bayesian inference on edge hardware*, develops specialised architectures; memristors, ferroelectric transistors, compute-in-memory chips; for probabilistic computation at the hardware level. These approaches remain in the hardware research domain and are not applicable to software deployment on commodity smartphones.

The third thread, *Bayesian deep learning*, integrates uncertainty into neural networks via MC-Dropout [Gal and Ghahramani, 2016], Bayes-by-Backprop [Blundell et al., 2015], or variational inference [Blei et al., 2017]. These methods require modified training procedures and iterative inference, increasing computational cost beyond what edge devices can accommodate.

Our contribution sits at the intersection of these three threads. To our knowledge, TinyBayes is the first framework to bring closed-form Bayesian inference; with principled uncertainty quantification and sub-kilobyte model size; to edge-deployable crop disease classification. We apply the Jacobi prior [Das and Dey, 2006, Das, 2008, Das and Sardar, 2025], which places a conjugate prior on the canonical parameter of the exponential family likelihood and yields a closed form, non-iterative posterior mode estimator via projection. Combined with YOLOv8-Nano for detection and MobileNetV3-Small for feature extraction, the complete pipeline fits in 9.5 MB and runs in 150 ms on a single CPU core.

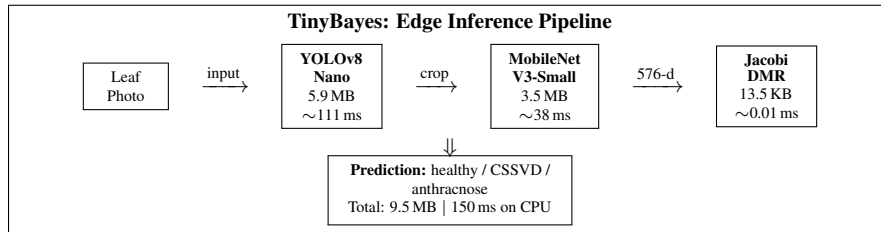


Figure 1: TinyBayes end-to-end inference pipeline: component sizes, latencies, and total CPU time.

Our contributions are:

- We present the first edge-deployable Bayesian pipeline for crop disease classification, combining YOLOv8-Nano (5.9 MB), MobileNetV3-Small (3.5 MB), and Jacobi-DMR (13.5 KB) for a total of 9.5 MB.
- We benchmark the Jacobi-DMR against seven classifiers on 576-dimensional MobileNetV3 features, showing competitive accuracy (78.7%) with the fastest training (0.06 s) and smallest model size.
- We demonstrate that the Jacobi-GP variant achieves the highest accuracy (86%) among all methods, serving as a theoretical upper bound for the Jacobi framework’s capacity.
- We provide a PCA ablation study across all eight classifiers, showing that dimensionality reduction via PCA does not offer any significant benefit while adding 450 KB of storage overhead; validating the use of all 576 raw features.
- We proved asymptotic consistency, asymptotic normality, bias correction and a finite-sample hyperparameter invariance property of the Jacobi-DMR estimator in Section 3.

2 The Jacobi Prior

Here we present the Jacobi prior framework briefly; while full details are in Das and Dey [2006], Das [2008], Das and Sardar [2025]. It presents the closed form analytical estimator for the regression coefficient for β .

Generalised Linear Model Setup Consider data $\mathcal{D} = \{(y_i, \mathbf{x}_i) \mid i = 1, \dots, n\}$ where y_i follows an exponential family distribution with canonical parameter θ_i , link function $g(\cdot)$, and linear predictor $\eta_i = \mathbf{x}_i' \beta$. Standard Bayesian inference places a prior $\pi(\beta)$ on the regression coefficients, yielding a posterior that requires expensive high-dimensional integration or iterative optimisation.

Prior on Canonical Parameters The Jacobi prior instead assigns a conjugate prior $\pi(\theta_i)$ to each canonical parameter. Since $g(\cdot)$ is one-to-one with Jacobian $J = |g'(\eta_i)|$, the posterior of η_i is $q(\eta_i | y_i) = \pi(g(\eta_i) | y_i) \cdot J$, and its mode $\hat{\eta}_i = h(y_i)$ is available in closed form.

Jacobi Estimator via Projection The vector $\hat{\boldsymbol{\eta}} = (h(y_1), \dots, h(y_n))'$ is projected onto the column space of \mathbf{X} :

$$\hat{\beta} = (\mathbf{X}'\mathbf{X})^{-1} \mathbf{X}' \hat{\boldsymbol{\eta}}. \quad (1)$$

This is a least-squares projection that decomposes $h(\mathbf{y}) = \mathbf{P}h(\mathbf{y}) + (\mathbf{I} - \mathbf{P})h(\mathbf{y})$, where $\mathbf{P} = \mathbf{X}(\mathbf{X}'\mathbf{X})^{-1} \mathbf{X}'$ is the linear transformation matrix representing the orthogonal projection from n -dimensional space \mathbb{R}^n onto the estimation space, while $(\mathbf{I} - \mathbf{P})$ represents the orthogonal projection of \mathbb{R}^n onto the error space.

Jacobi Estimator for Distributed Multinomial Regression (DMR) Following Taddy [2015], multinomial classification with K classes is handled via a Poisson surrogate representation. Although the observed responses satisfy $Y_{ik} \in \{0, 1\}$ with $\sum_{k=1}^K Y_{ik} = 1$, the DMR formulation treats each class k as arising from a Poisson regression with rate λ_{ik} . This is a working model; under a log-linear parameterisation, the Poisson likelihood yields the same score equations as the multinomial model [Taddy, 2015], leading to consistent estimation of the multinomial parameters despite the distributional mismatch. Placing the conjugate prior $\lambda_{ik} \sim \text{Gamma}(a_n, b_n)$ (rate parameterisation) under this working model, the Jacobi posterior mode for each class k is $\hat{\eta}_{ik} = \ln\left(\frac{y_{ik} + a}{1 + kb}\right)$, and the class-specific coefficient vector is $\hat{\beta}_k = (\mathbf{X}'\mathbf{X})^{-1} \mathbf{X}' \hat{\boldsymbol{\eta}}_k$. Prediction assigns $\text{argmax}_k \exp(\mathbf{x}'_{\text{new}} \hat{\beta}_k)$.

Gaussian Process Extension For nonlinear boundaries, the linear predictor is augmented with a GP random effect: $\eta_i = \mathbf{x}_i' \beta + w_i + \varepsilon_i$, where $w_i \sim \mathcal{GP}(0, \Sigma)$ with squared exponential kernel. The Jacobi-estimated $\hat{\boldsymbol{\eta}}$ serves as the GP's target, providing a closed-form initialisation for the nonparametric component.

3 Theoretical Results

We extend the asymptotic theory of the Jacobi estimator for Generalised Linear Models [Das and Sardar, 2025, Theorem 2.3] to the Jacobi-DMR of Section 2.

Model and estimator. Following Taddy [2015] and Das and Sardar [2025, Section 3.4], under the DMR Poisson surrogate, the multinomial classification problem with K classes is decomposed into K independent Poisson regressions:

$$Y_{ik} \sim \text{Poisson}(\lambda_{0,ik}), \quad \eta_{0,ik} = \log \lambda_{0,ik} = \mathbf{x}_i^\top \beta_{0,k}, \quad i = 1, \dots, n, \quad k = 1, \dots, K.$$

Placing the conjugate prior $\lambda_{ik} \sim \text{Gamma}(a_n, b_n)$ (rate parameterisation) on each λ_{ik} , the closed-form posterior mode of η_{ik} is

$$\hat{\eta}_{ik} = \log \frac{Y_{ik} + a_n}{1 + b_n}, \quad \hat{\beta}_k^{(n)} = (\mathbf{X}^\top \mathbf{X})^{-1} \mathbf{X}^\top \hat{\boldsymbol{\eta}}_k, \quad \hat{\boldsymbol{\eta}}_k = (\hat{\eta}_{1k}, \dots, \hat{\eta}_{nk})^\top.$$

Let $\tilde{\beta}_k^{(n)}$ denote the posterior mode of β_k under the induced Jacobi prior $\pi_J^{(k)}$. Define the stacked Jacobi-DMR estimator as $\hat{\beta}^{(n)} = ((\hat{\beta}_1^{(n)})^\top, \dots, (\hat{\beta}_K^{(n)})^\top)^\top \in \mathbb{R}^{Kp}$, and analogously define $\tilde{\beta}^{(n)}$ and β_0 .

Assumptions. For each $k \in \{1, \dots, K\}$:

- (B1) The Poisson log-likelihood $\ell_k(y, \eta) = y \eta - e^\eta$ is twice continuously differentiable in η , and the design matrix $\mathbf{X} \in \mathbb{R}^{n \times p}$ has full column rank p .
- (B2) The induced Jacobi prior $\pi_J^{(k)}(\boldsymbol{\beta}_k)$ on $\boldsymbol{\beta}_k$ and the prior $\pi_n^{(k)}(\boldsymbol{\eta}_k)$ on $\boldsymbol{\eta}_k$ are continuous and strictly positive on ε -balls around $\boldsymbol{\beta}_{0,k}$ and $\boldsymbol{\eta}_{0,k} = \mathbf{X}\boldsymbol{\beta}_{0,k}$, respectively.
- (B3) The normalised log-likelihood satisfies a uniform law of large numbers,

$$\sup_{\boldsymbol{\beta}_k \in \mathcal{B}} \left| \frac{1}{n} \sum_{i=1}^n \ell_k(Y_{ik}, \mathbf{x}_i^\top \boldsymbol{\beta}_k) - \mathbb{E}[\ell_k(Y_{1k}, \mathbf{x}_1^\top \boldsymbol{\beta}_k)] \right| \xrightarrow{P} 0.$$

- (B4) $Q_k(\boldsymbol{\beta}_k) := \mathbb{E}[\ell_k(Y_{1k}, \mathbf{x}_1^\top \boldsymbol{\beta}_k)]$ admits a unique maximiser $\boldsymbol{\beta}_{0,k} \in \mathbb{R}^p$, and $\boldsymbol{\eta}_{0,k} = \mathbf{X}\boldsymbol{\beta}_{0,k}$ uniquely maximises $R_k(\boldsymbol{\eta}_k) := \mathbb{E}[\ell_k(Y_{1k}, \boldsymbol{\eta}_k)]$.
- (B5) The hyperparameters scale as $a_n = b_n = 1/n$.
- (B6) (*Taddy DMR Poisson surrogate.*) $\{Y_{ik}\}_{i,k}$ are mutually independent across i and across k , with $Y_{ik} \sim \text{Poisson}(\exp(\mathbf{x}_i^\top \boldsymbol{\beta}_{0,k}))$.

Theorem 1 (Asymptotic Equivalence and Consistency). *Under Assumptions (B1)–(B6):*

- (i) For each $k = 1, \dots, K$, $\hat{\boldsymbol{\beta}}_k^{(n)} \xrightarrow{P} \boldsymbol{\beta}_{0,k}$, $\tilde{\boldsymbol{\beta}}_k^{(n)} \xrightarrow{P} \boldsymbol{\beta}_{0,k}$ ($n \rightarrow \infty$).
- (ii) For each k and every $\varepsilon, \delta > 0$ there exists an integer $N_k(\varepsilon, \delta)$ such that for all $n \geq N_k(\varepsilon, \delta)$, $P(\|\hat{\boldsymbol{\beta}}_k^{(n)} - \tilde{\boldsymbol{\beta}}_k^{(n)}\| > \varepsilon) < \delta$.
- (iii) Jointly, $\hat{\boldsymbol{\beta}}^{(n)} \xrightarrow{P} \boldsymbol{\beta}_0$ in \mathbb{R}^{Kp} , and for every $\varepsilon, \delta > 0$ there exists an integer $N(\varepsilon, \delta)$ such that for all $n \geq N(\varepsilon, \delta)$, $P(\|\hat{\boldsymbol{\beta}}^{(n)} - \tilde{\boldsymbol{\beta}}^{(n)}\| > \varepsilon) < \delta$. *Proof in Appendix 11*

Corollary 1 (Hyperparameter Invariance). *Suppose the targets are one-hot encoded: $Y_{ik} \in \{0, 1\}$ for all i, k with $\sum_{k=1}^K Y_{ik} = 1$. For any $a > 0$ and $b > 0$, the Jacobi-DMR predicted class*

$$\hat{C}(\mathbf{x}; a, b) := \arg \max_{k \in \{1, \dots, K\}} \mathbf{x}^\top \hat{\boldsymbol{\beta}}_k(a, b), \text{ where}$$

$$\hat{\boldsymbol{\beta}}_k(a, b) = (\mathbf{X}^\top \mathbf{X})^{-1} \mathbf{X}^\top \hat{\boldsymbol{\eta}}_k(a, b), \quad \hat{\eta}_{ik}(a, b) = \log \frac{Y_{ik} + a}{1 + b},$$

is invariant to (a, b) as the transformation induces a class(k)-independent shift and a common positive scaling of class scores, preserving the argmax decision intact. *Appendix 11.*

Remark 1. *Corollary 1 is a finite-sample, distribution-free property; which is consistent with Theorem 1: the coefficient vector $\hat{\boldsymbol{\beta}}_k(a, b)$ does depend on (a, b) , and only the consistent choice $a_n = b_n = 1/n$ delivers $\hat{\boldsymbol{\beta}}_k^{(n)} \xrightarrow{P} \boldsymbol{\beta}_{0,k}$. The argmax decision, however, is invariant in (a, b) for the Jacobi DMR framework.* *Appendix 11.*

Remark 2 (Empirical Validation). *We evaluated Jacobi-DMR over a grid of $(a, b) \in \{1/2000, 0.01, 0.05, 0.1, 0.2, 0.5, 1.0\}^2$ using all 576 features and found classification accuracy is invariant across the entire grid at 78.7%, consistent with Corollary 1.* *Appendix 11.*

Asymptotic normality under a high-intensity regime. To analyse the distribution of the Jacobi-DMR estimator, we introduce a high-intensity scaling of the Poisson surrogate. Specifically, we consider a sequence of models in which the Poisson rates are rescaled as $\lambda_{0,ik}^{(n)} = s_n \exp(\mathbf{x}_i^\top \boldsymbol{\beta}_{0,k})$, with $s_n \rightarrow \infty$. This scaling can be interpreted as an aggregation or exposure regime, where each observation represents s_n replicated events. Under this regime, the normalised fluctuation $\frac{Y_{ik} - \lambda_{0,ik}^{(n)}}{\lambda_{0,ik}^{(n)}}$ vanishes in probability, ensuring that the log-transformed responses admit a second-order linear

approximation. This linearisation is the key step enabling a central limit theorem for the projected estimator. It is important to note that this regime is not intrinsic to one-hot classification data, where $Y_{ik} \in \{0, 1\}$ and the implied rates are bounded. Rather, it serves as a theoretical device for characterising the estimator’s asymptotic behaviour. The practically relevant bounded-rate setting is addressed separately via bias correction in Remark 3.

Additional assumptions.

(C1) (*Large-rate regime.*) There exists a sequence $\lambda_{\min, n} \rightarrow \infty$ with $\lambda_{\min, n} = \omega(\sqrt{n})$ such that

$$\inf_{1 \leq i \leq n, 1 \leq k \leq K} \lambda_{0, ik} = \inf_{i, k} \exp(\mathbf{x}_i^\top \beta_{0, k}) \geq \lambda_{\min, n} \quad \text{for all sufficiently large } n.$$

(C2) (*Hyperparameter rate.*) $a_n, b_n \rightarrow 0$ with $\sqrt{n}(a_n + b_n) \rightarrow 0$. In particular, $a_n = b_n = 1/n$ satisfies this.

(C3) (*Design Gram limit.*) $n^{-1} \mathbf{X}^\top \mathbf{X} \rightarrow \mathbf{Q}$ for some positive-definite $\mathbf{Q} \in \mathbb{R}^{p \times p}$.

(C4) (*Lindeberg condition.*) $\max_{1 \leq i \leq n} \|\mathbf{x}_i\|^2/n \rightarrow 0$, and the triangular array $\{\mathbf{x}_i (Y_{ik} - \lambda_{0, ik})/\lambda_{0, ik}\}_{i=1}^n$ satisfies the Lindeberg condition for each k . (A sufficient condition is $\sup_i \|\mathbf{x}_i\| < \infty$.)

Theorem 2 (Asymptotic Normality). *Under Assumptions (B1)–(B6) and (C1)–(C4), for each $k = 1, \dots, K$, $\sqrt{n}(\hat{\beta}_k^{(n)} - \beta_{0, k}) \xrightarrow{d} \mathcal{N}(\mathbf{0}, \mathbf{Q}^{-1} \mathbf{V}_k \mathbf{Q}^{-1})$, where $\mathbf{V}_k := \lim_{n \rightarrow \infty} \frac{1}{n} \sum_{i=1}^n \mathbf{x}_i \mathbf{x}_i^\top e^{-\mathbf{x}_i^\top \beta_{0, k}}$. For the stacked estimator $\hat{\beta}^{(n)} \in \mathbb{R}^{Kp}$, $\sqrt{n}(\hat{\beta}^{(n)} - \beta_0) \xrightarrow{d} \mathcal{N}(\mathbf{0}, \Sigma)$, where $\Sigma \in \mathbb{R}^{Kp \times Kp}$ is the block-diagonal matrix with k -th diagonal block $\mathbf{Q}^{-1} \mathbf{V}_k \mathbf{Q}^{-1}$. The block-diagonal structure follows from the cross-class independence in Assumption (B6). Appendix 11.*

Remark 3 (Bias correction in the moderate-rate regime). *When the large-rate condition (C1) is replaced by the moderate-rate condition $\inf_{i, k} \lambda_{0, ik} \geq \lambda_{\min} > 0$ (rates bounded away from zero but not necessarily divergent), the Anscombe-type bias $-1/(2\lambda_{0, ik})$ no longer vanishes asymptotically, and the centring in Theorem 2 requires a correction. Define the bias-corrected Jacobi-DMR estimator*

$$\hat{\beta}_k^{(n, \text{bc})} := \hat{\beta}_k^{(n)} + \frac{1}{2} (\mathbf{X}^\top \mathbf{X})^{-1} \mathbf{X}^\top \left(e^{-\mathbf{x}_i^\top \hat{\beta}_k^{(n)}} \right)_{i=1}^n.$$

Under Assumptions (B1)–(B6), (C2)–(C4) and the moderate-rate condition, an analogous Taylor argument together with the consistency $\hat{\beta}_k^{(n)} \xrightarrow{P} \beta_{0, k}$ (Theorem 1) yields

$$\sqrt{n}(\hat{\beta}_k^{(n, \text{bc})} - \beta_{0, k}) \xrightarrow{d} \mathcal{N}(\mathbf{0}, \mathbf{Q}^{-1} \mathbf{V}_k \mathbf{Q}^{-1}).$$

The correction is an explicit, closed-form post-processing of $\hat{\beta}_k^{(n)}$ requiring no additional iterative computation, therefore preserves the edge-deployability of the Jacobi-DMR pipeline. Appendix 11.

4 Dataset

The Amini Cocoa Contamination Challenge [Amini and Zindi, 2024] provides annotated cocoa leaf images from West African farms with three class labels: **healthy**, **CSSVD** (chlorotic patches and vein banding from viral infection), and **anthracnose** (necrotic lesions from *Colletotrichum gloeosporioides*). Via stratified sampling with fixed random seeds, we constructed a **training set** of 2,000 balanced images (667/667/666 per class) and a disjoint **validation set** of 500 images (167/166/167 per class).

5 Methodology for Edge Deployment

Our pipeline has three stages, each designed for edge deployment. Figure 1 illustrates the complete inference flow.

Stage 1: Lesion Localisation via YOLOv8-Nano. We trained YOLOv8-Nano [Jocher et al., 2023], a 5.9 MB object detector designed for mobile devices, on the training set bounding box annotations for 10 epochs (batch size 16, image size 640×640 , Adam optimiser). At inference, boxes with confidence > 0.25 are retained. This replaces the Faster R-CNN used in prior work [Das and Sardar, 2025].

Stage 2: Feature Extraction via MobileNetV3-Small. A pretrained MobileNetV3-Small [Howard et al., 2019] (3.5 MB, ImageNet weights) serves as a fixed feature extractor. The classifier head is replaced with an identity mapping, yielding 576-dimensional feature vectors from each bounding box crop resized to 224×224 . All 576 features are retained without dimensionality reduction.

Stage 3: Classification. We evaluate eight classifiers on the extracted features: **Random Forest (RF)** (100 trees, all 576 features); **SVM** (RBF kernel, $C = 1.0$, $\gamma = \text{scale}$, standardised features); **Ridge** ($\alpha = 1.0$, standardised features); **Lasso** (L1-penalised logistic regression, SAGA solver, $C = 1.0$); **Elastic Net** (L1 ratio = 0.5, SAGA solver, $C = 1.0$); **XGBoost** (100 trees, max depth 6, learning rate 0.1); **Jacobi-DMR** (Distributed Multinomial Regression with $a = b = 1/n = 1/2000$, the consistent choice per Das and Sardar [2025]); **Jacobi-GP** (Gaussian Process regression on Jacobi-estimated targets, RBF kernel, $a = b = 1/2000$).

6 Empirical Results

6.1 Predictive Accuracy

Classification Performance Table 1 presents the comprehensive results for all eight classifiers on 576-dimensional MobileNetV3 features.

Table 1: Classification performance on the validation set. E2E Pred includes YOLOv8-Nano detection + MobileNetV3 feature extraction + classifier prediction, measured on CPU.

Method	Acc	M-P	M-R	M-F1	Train(s)	E2E Pred(ms)	Classifier Size	Edge?
Random Forest	0.732	0.737	0.733	0.732	5.23	140.7	4.4 MB	△
SVM (RBF)	0.818	0.819	0.818	0.818	1.22	135.2	6.5 MB	△
XGBoost	0.794	0.796	0.795	0.793	11.64	134.8	990.5 KB	△
Ridge	0.781	0.781	0.781	0.781	0.15	134.1	6.8 KB	✓
Lasso	0.785	0.785	0.785	0.784	83.19	134.1	6.8 KB	✓
Elastic Net	0.772	0.773	0.772	0.771	81.77	134.1	6.8 KB	✓
Jacobi-DMR	0.787	0.786	0.787	0.787	0.06	133.9	13.5 KB	✓
Jacobi-GP	<u>0.861</u>	<u>0.861</u>	<u>0.862</u>	<u>0.861</u>	295.46	151.4	104.9 MB	×

✓ Edge suitable △ Moderate × Not suitable

Jacobi-GP achieves the highest accuracy (86.1%) with perfect training fit, demonstrating nonlinear capacity. Among the edge-suitable models, Jacobi-DMR delivers the best macro F1 (0.787), fastest training (0.06 s), fastest inference (133.9 ms), and smallest classifier size (13.5 KB).

Table 2: Confusion matrices for selected classifiers. Rows: true class; Columns: predicted class.

	SVM			Jacobi-DMR			Jacobi-GP		
	H	C	A	H	C	A	H	C	A
H (184)	153	16	15	138	27	19	156	15	13
C (174)	20	137	17	22	136	16	14	148	12
A (176)	16	13	147	19	11	146	9	11	156

PCA Ablation: Feature Dimensionality To evaluate whether dimensionality reduction benefits the pipeline, we compared all eight classifiers on PCA-reduced 100 components (explaining 88.6% of total variance) versus raw 576-dimensional features. Table 3 presents the results.

Table 3: Accuracy comparison: PCA Top-100 vs All 576 features.

Method	PCA-100	All 576	Diff	Winner
Random Forest	0.758	0.732	-0.026	PCA-100
SVM (RBF)	0.832	0.818	-0.013	PCA-100
Ridge	0.781	0.781	0.000	Tied
Lasso	0.792	0.785	-0.008	PCA-100
Elastic Net	0.796	0.772	-0.024	PCA-100
XGBoost	0.773	0.794	+0.021	All-576
Jacobi-DMR	0.781	0.787	+0.006	All-576
Jacobi-GP	0.848	0.861	+0.013	All-576

It is evident that the accuracy difference between the top 100 principal components and all 576 features is marginal (1–2%). Moreover, PCA requires storing a 576×100 projection matrix (450 KB) on the device. At inference, predicting with all 576 raw features requires only 1,728 multiplications per image (576 features \times 3 classes), compared to 57,900 for PCA (576 \times 100 projection + 100 \times 3 classification). We therefore recommend using all 576 features directly.

6.2 Edge Device Feasibility

Table 4 summarises the deployment profile.

Table 4: Edge deployment profile for the TinyBayes pipeline.

Component	Size / Time
YOLOv8-Nano (detection)	5.9 MB
MobileNetV3-Small (features)	3.5 MB
Jacobi-DMR (classifier)	13.5 KB
Total pipeline	9.5 MB
CPU inference (Intel Xeon, Colab)	150 ms/image
Estimated mobile ARM CPU	300–450 ms/image

The complete pipeline fits in under 10 MB and delivers real-time inference on a single CPU core. On a mobile ARM processor, we estimate 2–3 times higher latency due to architectural differences, remaining within real-time bounds (< 500 ms). The Jacobi-DMR classifier itself contributes only 13.5 KB; making it negligible relative to the shared feature extraction pipeline.

7 Discussion

Closed-form Bayesian inference for edge-deployable agricultural systems. Existing edge-deployable agricultural systems [Malche et al., 2026] and [Khan et al., 2023] provide point predictions without uncertainty estimates. Bayesian methods that quantify uncertainty—MC-Dropout [Gal and Ghahramani, 2016], Bayes-by-Backprop [Blundell et al., 2015], variational inference [Blei et al., 2017]—require iterative inference incompatible with edge constraints. Hardware-level Bayesian inference operates in a different domain entirely. TinyBayes occupies a distinct point in this design space: analytical Bayesian inference at kilobyte scale (13.5 KB, zero iterative computation), integrated with an edge-deployable pipeline. To our knowledge, this combination has not been previously demonstrated for edge-device classification, particularly in agricultural disease detection.

What happens when a farmer photographs a leaf. At inference, the pipeline operates entirely on-device with no internet connectivity. The farmer captures a photograph of a cocoa leaf using their smartphone camera. YOLOv8-Nano processes the image (~ 111 ms on CPU) and outputs a bounding box around the disease-affected region. The cropped region is resized to 224×224 and passed through MobileNetV3-Small (~ 39 ms), producing a 576-dimensional feature vector. Finally, Jacobi-DMR computes three dot products; $\lambda_k = \exp(\mathbf{x}'\hat{\beta}_k)$ for $k \in \{\text{healthy, CSSVD, anthracnose}\}$; and returns

$\operatorname{argmax}_k \lambda_k$ as the prediction (~ 0.01 ms). The entire process completes in ~ 150 ms. Crucially, the YOLO and MobileNetV3 components account for 99.99% of inference time; the Jacobi-DMR classifier contributes effectively zero latency. This means that any improvement to the shared feature extraction pipeline (e.g., faster hardware, model quantisation) directly reduces end-to-end latency, while the Bayesian classifier remains a negligible overhead.

Jacobi-DMR vs Jacobi-GP: the deployment trade-off. Jacobi-GP achieves the highest accuracy (86.1%) but is unsuitable for edge deployment: it requires storing all $n = 2,000$ training points (~ 27 MB) and ~ 3.5 million operations per image, versus 13.5 KB and 1,728 multiplications for Jacobi-DMR. Both methods share the same Bayesian foundation (closed-form $\hat{\eta}$ via the Jacobi prior), differing only in projection: linear (DMR) versus nonparametric (GP). Jacobi-GP serves as a theoretical upper bound, whereas Jacobi-DMR is the practical deployment choice.

Why not Ridge, Lasso, or Elastic Net? These methods achieve comparable accuracy (77–78%) and similar classifier sizes (~ 7 KB), but have three disadvantages. First, they do not offer uncertainty quantification; Jacobi-DMR supports posterior sampling via an efficient parallel Monte Carlo algorithm [Das and Sardar, 2025] without iterative optimisation. Second, they require feature standardisation at inference which requires storage of scaling parameters, whereas Jacobi-DMR operates on raw features directly. Third, Lasso and Elastic Net require iterative SAGA optimisation (83 s and 82 s respectively) versus Jacobi-DMR’s single matrix operation (0.06 s).

Rapid retraining for evolving diseases. While training time does not affect edge inference, Jacobi-DMR’s sub-second training enables rapid model updates; a critical advantage for agricultural deployment. When new labelled samples become available for existing disease categories, only the Jacobi coefficient vectors require recomputation via the closed-form projection $\hat{\beta} = (\mathbf{X}'\mathbf{X})^{-1}\mathbf{X}'\hat{\eta}$, while the feature extraction pipeline (YOLOv8-Nano and MobileNetV3) remains fixed. For entirely new disease categories, a single additional coefficient vector is computed without modifying any other component. This modularity makes TinyBayes uniquely suited to agricultural settings where new disease variants, regional variations, or seasonal changes demand frequent model updates with minimal computational overhead.

Extending the Jacobi prior to edge-deployable systems. Das and Sardar [2025] demonstrated the Jacobi prior on server-grade pipelines with no deployment constraints, demonstrating the Jacobi prior on SDSS astronomical data, US SBA loan defaults, and RSNA lumbar spine MRI classification using ResNet-50 features. The cocoa leaf disease task differs in domain (agriculture), imaging modality (field photographs), and deployment constraints (edge devices); to our knowledge, no prior work integrates these aspects within a Bayesian closed form solution framework.

8 Related Work

Plant disease detection on edge. Khan et al. [2023] deployed MobileNetV3 for plant disease classification on the PlantVillage dataset, achieving strong accuracy but without any Bayesian component. The MSDFEN framework [Dai et al., 2025] combines dynamic multi-scale feature extraction with lightweight architectures, but does not explicitly model predictive uncertainty.

Bayesian methods for classification. The Horseshoe prior [Carvalho et al., 2010] and Bayesian Lasso [Park and Casella, 2008] require MCMC sampling. Variational inference [Blei et al., 2017] and MC-Dropout [Gal and Ghahramani, 2016] offer faster alternatives but still involve iterative computation. UniLasso [Chatterjee et al., 2025] provides a novel approach to sparse regression but does not natively support multinomial classification. The Jacobi prior is unique in providing a non-iterative, closed-form Bayesian estimator for multinomial classification via the DMR decomposition.

Efficient classifiers on deep features. Using pretrained CNNs as feature extractors followed by classical classifiers is well-established [Razavian et al., 2014]. Our contribution is demonstrating that the Jacobi prior provides the best accuracy–efficiency trade-off in this paradigm for edge-deployable agricultural imaging, with the added benefit of Bayesian uncertainty quantification.

9 Limitations

The validation set (500 samples) is relatively small; larger-scale evaluation would strengthen the conclusions. The Jacobi-GP’s $\mathcal{O}(n^3)$ complexity limits its use to server-side inference. We used pretrained (non-fine-tuned) MobileNetV3 features; domain-specific fine-tuning would likely improve all classifiers. CPU inference was benchmarked on an Intel Xeon (Colab); actual mobile inference assumed to be 2–3 times slower (see Table 4). The dataset contains only three classes; extending to finer-grained severity grading remains future work.

10 Conclusion

We have introduced TinyBayes, a complete edge-deployable pipeline for cocoa disease classification that combines YOLOv8-Nano (5.9 MB), MobileNetV3-Small (3.5 MB), and the Jacobi-DMR classifier (13.5 KB) into a 9.5 MB system that runs in 150 ms on a single CPU core. The Jacobi-DMR achieves 78.7% accuracy while being the fastest classifier to train (0.06 s) and the smallest to store; yet it is the only method in our comparison that supports Bayesian uncertainty quantification, via the closed-form Monte Carlo algorithm of Das and Sardar [2025], without iterative computation. The Jacobi-GP variant achieves the highest accuracy (86.1%), demonstrating that the Jacobi framework’s capacity extends to nonlinear decision boundaries when server-side resources are available.

Three properties distinguish TinyBayes from existing approaches. First, its modularity: only the 13.5 KB coefficient vectors require updating when new disease samples or categories arise, while the detection and feature extraction stages remain fixed, unless absolutely required. Second, its hyperparameter invariance: the classifier requires no tuning, a practical advantage over Ridge, Lasso, and Elastic Net which demand cross-validation. Third, its Bayesian foundation: unlike all frequentist alternatives of comparable size, Jacobi-DMR provides calibrated prediction intervals that inform downstream decision-making; critical in agricultural contexts where a misclassification can trigger unnecessary or delayed intervention.

Beyond cocoa, the TinyBayes architecture generalises to any image classification task where a lightweight detector, a pretrained feature extractor, and a linear Bayesian classifier can be composed. We believe this paradigm; a closed-form Bayesian inference under 10 MB total size; opens a practical path toward uncertainty-aware AI on commodity devices in resource-constrained settings worldwide.

11 Broader Impact

Cocoa farming sustains the livelihoods of approximately two million smallholder families in West Africa, many of whom lack access to trained agricultural extension officers for timely disease diagnosis. TinyBayes addresses this gap by enabling real-time, on-device disease detection that requires no internet connectivity and runs on entry-level smartphones - the most widely available computing platform in rural Sub-Saharan Africa. Early identification of CSSVD and anthracnose can prompt targeted intervention before disease spreads to neighbouring trees, potentially reducing crop losses that currently cost the industry billions of dollars annually.

By replacing server-dependent pipelines with a 9.5 MB on-device solution, TinyBayes eliminates cloud inference energy costs—a meaningful saving when scaled to millions of daily classifications across farming cooperatives.

We identify two risks: over-reliance on automated predictions (e.g., destroying a healthy tree misclassified as CSSVD-infected), mitigated by using TinyBayes as a decision-support tool alongside agricultural extension officers; and limited generalisation beyond the specific dataset of West African cocoa training region, mitigated by Jacobi-DMR’s sub-second retraining capability for regional adaptation.

References

- Amini and Zindi. Amini cocoa contamination challenge. <https://zindi.africa/competitions/amini-cocoa-contamination-challenge>, 2024.
- David M. Blei, Alp Kucukelbir, and Jon D. McAuliffe. Variational inference: A review for statisticians. *Journal of the American Statistical Association*, 112(518):859–877, 2017.
- Charles Blundell, Julien Cornebise, Koray Kavukcuoglu, and Daan Wierstra. Weight uncertainty in neural networks. In *International Conference on Machine Learning (ICML)*, pages 1613–1622, 2015.
- Carlos M. Carvalho, Nicholas G. Polson, and James G. Scott. The horseshoe estimator for sparse signals. *Biometrika*, 97(2):465–480, 2010.
- Sourav Chatterjee, Trevor Hastie, and Robert Tibshirani. Univariate-guided sparse regression. *Harvard Data Science Review*, 7(3), 2025.
- Zhiyuan Dai, Yuyang Jiang, Laiyuan Cao, Xiaojun Zhang, and Zhi Tao. Msdfen: Multi-scale dynamic feature extraction network for pathological voice detection. *Applied Acoustics*, 2025.
- Sourish Das. *Generalized Linear Models and Beyond: An Innovative Approach from Bayesian Perspective*. PhD thesis, University of Connecticut, 2008.
- Sourish Das and Dipak K. Dey. On Bayesian analysis of generalized linear models using the Jacobian technique. *The American Statistician*, 60(3):264–268, 2006.
- Sourish Das and Shouvik Sardar. Jacobi prior: An alternative Bayesian method for supervised learning. *arXiv preprint arXiv:2404.11345*, 2025. Under review.
- G. A. Dzahini-Obiatey, O. Domfeh, and F. M. Amoah. Over seventy years of a viral disease of cocoa in Ghana: From researchers’ perspective. *African Journal of Agricultural Research*, 5(7):476–485, 2010.
- Yarin Gal and Zoubin Ghahramani. Dropout as a Bayesian approximation: Representing model uncertainty in deep learning. In *International Conference on Machine Learning (ICML)*, pages 1050–1059, 2016.
- Andrew Howard, Mark Sandler, Grace Chu, Liang-Chieh Chen, Bo Chen, Mingxing Tan, Weijun Wang, Yukun Zhu, Ruoming Pang, Vijay Vasudevan, Quoc V. Le, and Hartwig Adam. Searching for MobileNetV3. In *IEEE/CVF International Conference on Computer Vision (ICCV)*, pages 1314–1324, 2019.
- International Cocoa Organization. Quarterly bulletin of cocoa statistics. *ICCO*, 2023.
- Glenn Jocher, Ayush Chaurasia, and Jing Qiu. Ultralytics YOLOv8. <https://github.com/ultralytics/ultralytics>, 2023.
- Ameer Tamoor Khan, Signe Marie Jensen, Abdul Rehman Khan, and Shuai Li. Plant disease detection model for edge computing devices. *Frontiers in Plant Science*, 2023.
- Timothy Malche, Mukesh Joshi, Govind Murari Upadhyay, and Pramod Kumar Soni. Automated tomato leaf disease detection and alert system using internet of things and tinyml. *Discover Internet of Things*, 2026.
- J. P. Marelli, D. R. Guest, B. A. Bailey, H. C. Evans, J. K. Brown, M. Goss, A. Crozier, and N. Bainbridge. Chocolate under threat from old and new cacao diseases. *Phytopathology*, 109(8): 1331–1343, 2019.
- Sharada P. Mohanty, David P. Hughes, and Marcel Salathé. Using deep learning for image-based plant disease detection. *Frontiers in Plant Science*, 7:1419, 2016.
- Trevor Park and George Casella. The Bayesian Lasso. *Journal of the American Statistical Association*, 103(482):681–686, 2008.

Ali Sharif Razavian, Hossein Azizpour, Josephine Sullivan, and Stefan Carlsson. CNN features off-the-shelf: An astounding baseline for recognition. In *IEEE Conference on Computer Vision and Pattern Recognition Workshops*, pages 806–813, 2014.

Matt Taddy. Distributed multinomial regression. *The Annals of Applied Statistics*, 9(3):1394–1414, 2015.

Appendix

Proof of Theorem 1. : Fix $k \in \{1, \dots, K\}$. Following the construction of Das and Sardar [2025, Theorem 2.3], define the per-class objective in β_k -space by

$$Q_{n,k}(\beta_k) = \frac{1}{n} \sum_{i=1}^n \ell_k(Y_{ik}, \mathbf{x}_i^\top \beta_k) + \frac{1}{n} \log \pi_J^{(k)}(\beta_k),$$

so that $\tilde{\beta}_k^{(n)} = \arg \max_{\beta_k} Q_{n,k}(\beta_k)$, and the per-class objective in η_k -space by

$$R_{n,k}(\eta_k) = \frac{1}{n} \sum_{i=1}^n \ell_k(Y_{ik}, \eta_{ik}) + \frac{1}{n} \log \pi_n^{(k)}(\eta_k),$$

so that the per-observation maximisers $\hat{\eta}_{ik} = \arg \max_{\eta_{ik}} \log \pi_n^{(k)}(\eta_{ik} | Y_{ik})$ together form $\hat{\eta}_k = \arg \max_{\eta_k} R_{n,k}(\eta_k)$, with $\hat{\beta}_k^{(n)} = (\mathbf{X}^\top \mathbf{X})^{-1} \mathbf{X}^\top \hat{\eta}_k$.

Step 1 (vanishing prior contribution). By Assumption (B2), $\log \pi_J^{(k)}$ is continuous on $B_\varepsilon(\beta_{0,k})$. For any compact $K_1 \subset B_\varepsilon(\beta_{0,k})$, continuity yields a finite constant $M_{K_1} < \infty$ with $\sup_{\beta_k \in K_1} \log \pi_J^{(k)}(\beta_k) \leq M_{K_1}$, hence

$$\sup_{\beta_k \in K_1} \frac{1}{n} \left| \log \pi_J^{(k)}(\beta_k) \right| \leq \frac{M_{K_1}}{n} \xrightarrow{n \rightarrow \infty} 0. \quad (2)$$

For the conjugate Gamma(a_n, b_n) prior on λ_{ik} in rate form, the change of variables $\eta_{ik} = \log \lambda_{ik}$ together with the Jacobian $d\lambda_{ik}/d\eta_{ik} = e^{\eta_{ik}}$ yields the induced per-coordinate prior

$$\pi_n^{(k)}(\eta_{ik}) \propto \exp\{a_n \eta_{ik} - b_n e^{\eta_{ik}}\}, \quad (3)$$

up to an η_{ik} -free normalising constant. By independence across i ,

$$\frac{1}{n} \log \pi_n^{(k)}(\eta_k) = \frac{a_n}{n} \sum_{i=1}^n \eta_{ik} - \frac{b_n}{n} \sum_{i=1}^n e^{\eta_{ik}} + \text{const.}$$

For any compact $K_2 \subset B_\varepsilon(\eta_{0,k})$ there exist finite constants $M_1, M_2 < \infty$ such that $\sup_{\eta_k \in K_2} \max_i |\eta_{ik}| \leq M_1$ and $\sup_{\eta_k \in K_2} \max_i e^{\eta_{ik}} \leq M_2$. Hence under Assumption (B5) ($a_n = b_n = 1/n$),

$$\sup_{\eta_k \in K_2} \left| \frac{1}{n} \log \pi_n^{(k)}(\eta_k) \right| \leq a_n M_1 + b_n M_2 = \frac{M_1 + M_2}{n} \xrightarrow{n \rightarrow \infty} 0, \quad (4)$$

matching the prior-vanishing identity used in Equations (2.5)–(2.6) of Das and Sardar [2025] (cf. Remark 3.1 there).

Step 2 (uniform convergence of objectives). Combining (B3) with (2) and (4),

$$\sup_{\beta_k \in \mathcal{B}} |Q_{n,k}(\beta_k) - Q_k(\beta_k)| \xrightarrow{P} 0, \quad \sup_{\eta_k \in \mathcal{H}} |R_{n,k}(\eta_k) - R_k(\eta_k)| \xrightarrow{P} 0,$$

where $\mathcal{H} = \{\mathbf{X}\beta_k : \beta_k \in \mathcal{B}\}$.

Step 3 (argmax continuous mapping). By Assumption (B4), Q_k and R_k have unique maximisers at $\beta_{0,k}$ and $\eta_{0,k}$ respectively. Applying the argmax continuous mapping theorem to the convergence in Step 2 yields

$$\tilde{\beta}_k^{(n)} \xrightarrow{P} \beta_{0,k}, \quad \hat{\eta}_k \xrightarrow{P} \eta_{0,k} = \mathbf{X}\beta_{0,k}.$$

Step 4 (continuous projection). By (B1), \mathbf{X} has full column rank, so the linear map $\eta \mapsto (\mathbf{X}^\top \mathbf{X})^{-1} \mathbf{X}^\top \eta$ is well-defined and continuous. The continuous mapping theorem then gives

$$\hat{\beta}_k^{(n)} = (\mathbf{X}^\top \mathbf{X})^{-1} \mathbf{X}^\top \hat{\eta}_k \xrightarrow{P} (\mathbf{X}^\top \mathbf{X})^{-1} \mathbf{X}^\top \eta_{0,k} = \beta_{0,k}.$$

Combined with $\tilde{\beta}_k^{(n)} \xrightarrow{P} \beta_{0,k}$ from Step 3, this proves part (i).

Step 5 (asymptotic equivalence). Both $\hat{\beta}_k^{(n)}$ and $\tilde{\beta}_k^{(n)}$ converge in probability to the same limit $\beta_{0,k}$. By the triangle inequality, for every $\varepsilon > 0$,

$$\|\hat{\beta}_k^{(n)} - \tilde{\beta}_k^{(n)}\| \leq \|\hat{\beta}_k^{(n)} - \beta_{0,k}\| + \|\tilde{\beta}_k^{(n)} - \beta_{0,k}\|,$$

so for every $\delta > 0$,

$$P\left(\|\hat{\beta}_k^{(n)} - \tilde{\beta}_k^{(n)}\| > \varepsilon\right) \leq P\left(\|\hat{\beta}_k^{(n)} - \beta_{0,k}\| > \varepsilon/2\right) + P\left(\|\tilde{\beta}_k^{(n)} - \beta_{0,k}\| > \varepsilon/2\right).$$

Each summand is below $\delta/2$ for $n \geq N_k(\varepsilon, \delta)$ by part (i), establishing part (ii).

Step 6 (joint statement). By Assumption (B6), the per-class statements in (i)–(ii) are simultaneous. Using the Euclidean norm $\|\hat{\beta}^{(n)} - \tilde{\beta}^{(n)}\|^2 = \sum_{k=1}^K \|\hat{\beta}_k^{(n)} - \tilde{\beta}_k^{(n)}\|^2$, the event $\{\|\hat{\beta}^{(n)} - \tilde{\beta}^{(n)}\| > \varepsilon\}$ is contained in $\bigcup_{k=1}^K \{\|\hat{\beta}_k^{(n)} - \tilde{\beta}_k^{(n)}\| > \varepsilon/\sqrt{K}\}$, so a union bound gives

$$P\left(\|\hat{\beta}^{(n)} - \tilde{\beta}^{(n)}\| > \varepsilon\right) \leq \sum_{k=1}^K P\left(\|\hat{\beta}_k^{(n)} - \tilde{\beta}_k^{(n)}\| > \varepsilon/\sqrt{K}\right).$$

Applying part (ii) with δ/K to each summand yields the joint asymptotic equivalence in (iii). The joint convergence $\hat{\beta}^{(n)} \xrightarrow{P} \beta_0$ follows from (i) and the continuous mapping theorem applied to the stacking map. \square

Proof of Corollary 1. We show that the prediction rule is invariant to (a, b) by explicitly decomposing the transformed response and tracking its effect through the estimator.

Step 1: Response decomposition. For $Y_{ik} \in \{0, 1\}$,

$$\hat{\eta}_{ik}(a, b) = \log \frac{Y_{ik} + a}{1 + b} = \log(Y_{ik} + a) - \log(1 + b).$$

We now express $\log(Y_{ik} + a)$ in a form linear in Y_{ik} . Since $Y_{ik} \in \{0, 1\}$,

$$\log(Y_{ik} + a) = \begin{cases} \log(1 + a), & \text{if } Y_{ik} = 1, \\ \log(a), & \text{if } Y_{ik} = 0. \end{cases}$$

Hence,

$$\log(Y_{ik} + a) = \log(a) + Y_{ik} \cdot \log\left(\frac{1 + a}{a}\right).$$

Define

$$\gamma(a) := \log\left(\frac{1 + a}{a}\right) > 0.$$

Then

$$\hat{\eta}_{ik}(a, b) = \underbrace{(\log(a) - \log(1 + b))}_{=: c(a, b)} + \gamma(a) Y_{ik}.$$

In vector form,

$$\hat{\eta}_k(a, b) = c(a, b) \mathbf{1}_n + \gamma(a) \mathbf{Y}_k.$$

Step 2: Projection. Applying the closed-form estimator,

$$\hat{\beta}_k(a, b) = (\mathbf{X}^\top \mathbf{X})^{-1} \mathbf{X}^\top \hat{\eta}_k(a, b),$$

we obtain

$$\hat{\beta}_k(a, b) = c(a, b) \mathbf{v} + \gamma(a) \mathbf{w}_k,$$

where

$$\mathbf{v} := (\mathbf{X}^\top \mathbf{X})^{-1} \mathbf{X}^\top \mathbf{1}_n, \quad \mathbf{w}_k := (\mathbf{X}^\top \mathbf{X})^{-1} \mathbf{X}^\top \mathbf{Y}_k.$$

Step 3: Effect on prediction. For any $\mathbf{x} \in \mathbb{R}^p$,

$$\mathbf{x}^\top \hat{\beta}_k(a, b) = c(a, b) \mathbf{x}^\top \mathbf{v} + \gamma(a) \mathbf{x}^\top \mathbf{w}_k.$$

The first term does not depend on k and therefore cancels in the arg max. Since $\gamma(a) > 0$ for all $a > 0$, multiplication by $\gamma(a)$ preserves ordering across k . Hence,

$$\arg \max_k \mathbf{x}^\top \hat{\beta}_k(a, b) = \arg \max_k \mathbf{x}^\top \mathbf{w}_k,$$

which is independent of (a, b) . \square

Proof of Theorem 2. : Fix $k \in \{1, \dots, K\}$. Write $\eta_{0,ik} = \mathbf{x}_i^\top \beta_{0,k}$, $\lambda_{0,ik} = e^{\eta_{0,ik}}$, and $T_{ik} := (Y_{ik} - \lambda_{0,ik})/\lambda_{0,ik}$, so that $\mathbb{E}[T_{ik}] = 0$ and $\text{Var}(T_{ik}) = 1/\lambda_{0,ik} = e^{-\eta_{0,ik}}$. Then

$$\hat{\eta}_{ik} - \eta_{0,ik} = \log \frac{Y_{ik} + a_n}{(1 + b_n) \lambda_{0,ik}} = \log \left(1 + T_{ik} + \frac{a_n}{\lambda_{0,ik}} \right) - \log(1 + b_n).$$

Step 1 (Taylor expansion on a high-probability event). By Assumption (C1), $\lambda_{0,ik} \geq \lambda_{\min,n} \rightarrow \infty$ uniformly in i, k . By Bernstein concentration for centred Poisson variables, $P(|T_{ik}| > 1/2) \leq 2 \exp(-c \lambda_{0,ik}) \leq 2 \exp(-c \lambda_{\min,n})$ for an absolute constant $c > 0$. Letting $\mathcal{E}_n = \{ \max_{i,k} |T_{ik}| \leq 1/2 \} \cap \{ a_n/\lambda_{\min,n} \leq 1/4 \}$, a union bound gives $P(\mathcal{E}_n^c) \leq 2nK \exp(-c \lambda_{\min,n}) = o(n^{-1/2})$ under (C1). On \mathcal{E}_n , the second-order Taylor expansion of $u \mapsto \log(1 + u)$ around $u = 0$ yields

$$\hat{\eta}_{ik} - \eta_{0,ik} = T_{ik} + \underbrace{\frac{a_n}{\lambda_{0,ik}} - b_n}_{=: r_{ik}^{(1)}} - \frac{1}{2} \left(T_{ik} + \frac{a_n}{\lambda_{0,ik}} \right)^2 + r_{ik}^{(2)},$$

where $|r_{ik}^{(2)}| \leq C |T_{ik} + a_n/\lambda_{0,ik}|^3 + C b_n^2$ for an absolute constant C .

Step 2 (bias is asymptotically negligible). Taking expectations,

$$\mathbb{E}[\hat{\eta}_{ik} - \eta_{0,ik}] = -\frac{1}{2\lambda_{0,ik}} + \frac{a_n}{\lambda_{0,ik}} - b_n + O\left(\frac{1}{\lambda_{0,ik}^2} + a_n^2 + b_n^2\right).$$

Under (C1) and (C2),

$$\left\| \frac{1}{\sqrt{n}} \mathbf{X}^\top \mathbb{E}[\hat{\eta}_k - \eta_{0,k}] \right\| = O\left(\frac{\sqrt{n}}{\lambda_{\min,n}}\right) + O(\sqrt{n}(a_n + b_n)) = o(1),$$

since $\lambda_{\min,n} = \omega(\sqrt{n})$ by (C1) and $\sqrt{n}(a_n + b_n) \rightarrow 0$ by (C2).

Step 3 (leading stochastic term). The leading stochastic term in the expansion of Step 1 is T_{ik} , with $\mathbb{E}[T_{ik}] = 0$ and $\text{Var}(T_{ik}) = e^{-\eta_{0,ik}}$. By Assumption (C4) and the Lindeberg–Feller central limit theorem applied to the triangular array $\{\mathbf{x}_i T_{ik}\}_{i=1}^n$,

$$\frac{1}{\sqrt{n}} \mathbf{X}^\top \mathbf{T}_k = \frac{1}{\sqrt{n}} \sum_{i=1}^n \mathbf{x}_i T_{ik} \xrightarrow{d} \mathcal{N}(\mathbf{0}, \mathbf{V}_k), \quad \mathbf{V}_k = \lim_n \frac{1}{n} \sum_{i=1}^n \mathbf{x}_i \mathbf{x}_i^\top e^{-\mathbf{x}_i^\top \beta_{0,k}}.$$

Step 4 (remainders are negligible). The centred fluctuation of the second-order Taylor term has variance $O(\lambda_{0,ik}^{-2}) = o(\lambda_{\min,n}^{-2})$, so by Chebyshev's inequality

$$\frac{1}{\sqrt{n}} \sum_{i=1}^n \mathbf{x}_i \left[\frac{1}{2} \left(T_{ik} + \frac{a_n}{\lambda_{0,ik}} \right)^2 - \frac{1}{2} \mathbb{E} \left(T_{ik} + \frac{a_n}{\lambda_{0,ik}} \right)^2 \right] = o_P(1),$$

where the mean has been absorbed into the bias of Step 2. Similarly, the cubic remainder satisfies $n^{-1/2} \sum_i \mathbf{x}_i r_{ik}^{(2)} = o_P(1)$ on \mathcal{E}_n . Since $P(\mathcal{E}_n^c) = o(n^{-1/2})$, the contribution off \mathcal{E}_n is also $o_P(1)$.

Step 5 (combining and projecting). Steps 1–4 give the linearisation

$$\frac{1}{\sqrt{n}} \mathbf{X}^\top (\hat{\boldsymbol{\eta}}_k - \boldsymbol{\eta}_{0,k}) = \frac{1}{\sqrt{n}} \mathbf{X}^\top \mathbf{T}_k + o_P(1) \xrightarrow{d} \mathcal{N}(\mathbf{0}, \mathbf{V}_k).$$

By (C3), $(n^{-1} \mathbf{X}^\top \mathbf{X})^{-1} \rightarrow \mathbf{Q}^{-1}$, and Slutsky's theorem yields

$$\sqrt{n} (\hat{\boldsymbol{\beta}}_k^{(n)} - \boldsymbol{\beta}_{0,k}) = \left(\frac{\mathbf{X}^\top \mathbf{X}}{n} \right)^{-1} \cdot \frac{1}{\sqrt{n}} \mathbf{X}^\top (\hat{\boldsymbol{\eta}}_k - \boldsymbol{\eta}_{0,k}) \xrightarrow{d} \mathcal{N}(\mathbf{0}, \mathbf{Q}^{-1} \mathbf{V}_k \mathbf{Q}^{-1}).$$

Step 6 (joint distribution). By the cross-class independence in (B6), the per-class score vectors $n^{-1/2} \mathbf{X}^\top \mathbf{T}_k$ are mutually independent across k . Hence the joint limit is the product Gaussian, equivalent to $\mathcal{N}(\mathbf{0}, \boldsymbol{\Sigma})$ with $\boldsymbol{\Sigma}$ block-diagonal and k -th block $\mathbf{Q}^{-1} \mathbf{V}_k \mathbf{Q}^{-1}$. \square